



Cite this: *Chem. Sci.*, 2024, **15**, 15679

All publication charges for this article have been paid for by the Royal Society of Chemistry

Received 7th February 2024  
Accepted 23rd August 2024

DOI: 10.1039/d4sc00925h  
[rsc.li/chemical-science](http://rsc.li/chemical-science)

## Introduction

The ensemble of conformations a given molecule can access is of utmost importance, since each conformation defines a 3D shape, which in turn determines the molecule's physical, chemical and biological properties.<sup>1,2</sup> Thus, the exploration of conformational space, including the less abundant conformations, is a prerequisite to gain a deeper understanding of these properties.

As molecular geometry and function are interrelated, there has been growing interest in remodeling the conformational space and designing molecules that can adopt the desired shape with minimal or no energetic penalty. The common strategy that guided these efforts was to impose structural constraints *via* steric repulsion or ring strains. As a result of these challenging undertakings, peculiar reactivities,<sup>3</sup> well-designed emissive systems,<sup>4</sup> rarely observed metastable conformational and redox states<sup>5</sup> and enhanced ligand bindings<sup>6</sup> have been engineered.

<sup>a</sup>Centre for Structural Science, HUN-REN Research Centre for Natural Sciences, Magyar tudósok körùtja 2, H-1117 Budapest, Hungary. E-mail: domjan.attila@ttk.hu

<sup>b</sup>Institute of Organic Chemistry, HUN-REN Research Centre for Natural Sciences, Magyar tudósok körùtja 2, H-1117 Budapest, Hungary. E-mail: papai.imre@ttk.hu; soos.tibor@ttk.hu

<sup>c</sup>Hevesy György PhD School of Chemistry, Eötvös Loránd University, P. O. Box 32, Budapest, H-1518, Hungary

† Electronic supplementary information (ESI) available. CCDC 2004799 and 2004800. For ESI and crystallographic data in CIF or other electronic format see DOI: <https://doi.org/10.1039/d4sc00925h>

## Illuminating the multiple Lewis acidity of triaryl-boranes *via* atropisomeric dative adducts†

Benjámin Kovács,<sup>a</sup> Tamás Földes,<sup>b</sup> Márk Szabó,<sup>a</sup> Éva Dorkó,<sup>b</sup> Bianka Kótai,<sup>b</sup> Gergely Laczkó,<sup>b</sup> Tamás Holczbauer,<sup>b</sup> Attila Domján,<sup>a</sup> Imre Pápai,<sup>b</sup> and Tibor Soós<sup>a,b</sup>

Using the principle that constrained conformational spaces can generate novel and hidden molecular properties, we challenged the commonly held perception that a single-centered Lewis acid reacting with a single-centered Lewis base always forms a single Lewis adduct. Accordingly, the emergence of single-centered but multiple Lewis acidity among sterically hindered and non-symmetric triaryl-boranes is reported. These Lewis acids feature several diastereotopic faces providing multiple binding sites at the same Lewis acid center in the interaction with Lewis bases giving rise to adducts with diastereomeric structures. We demonstrate that with a proper choice of the base, atropisomeric adduct species can be formed that interconvert *via* the dissociative mechanism rather than conformational isomerism. The existence of this exotic and peculiar molecular phenomenon was experimentally confirmed by the formation of atropisomeric piperidine-borane adducts using state-of-the-art NMR techniques in combination with computational methods.

Along the above lines, we took up the challenge of demonstrating the existence of a peculiar molecular phenomenon that enables multiple Lewis acidity (MLA) to be assigned to a single-centered Lewis acid (LA). IUPAC defines Lewis acidity as '*the thermodynamic tendency of a substrate to act as a Lewis acid*'<sup>7</sup> which is routinely described by a single equilibrium constant associated with a single dative adduct. In contrast, we envisioned that sterically crowded and non-symmetric triaryl-boranes, *i.e.* those involving an LA center with diastereotopic faces and confinement,<sup>8</sup> are able to form distinct dative LA-LB adducts<sup>9</sup> with the same single-centered achiral Lewis base (LB). Accordingly, these Lewis adducts represent different stereoisomeric states formed in competitive association pathways. Due to hindered rotations around single bonds, these LA-LB stereoisomers are diastereomeric atropisomers, which can be distinguished at ambient temperature, and thus, the Lewis acidity of these boranes can be described by not a single, but multiple equilibrium constants. Atropisomerism is a unique case of stereoisomerism caused by restricted rotation around a single covalent bond that is not constrained in a ring. While this phenomenon commonly refers to  $C(sp^2)-C(sp^2)$  single bonds, there are some less common examples for atropisomerism as a result of restricted rotation around  $C(sp^3)-C(sp^2)$  or even  $C(sp^3)-C(sp^3)$  single bonds (see Fig. 1 for selected examples).<sup>10</sup> In this study we demonstrate that atropisomeric LA-LB adducts with dual restricted rotation around  $B(sp^3)-N(sp^3)$  and  $B(sp^3)-Ar(sp^2)$  bonds are formed between fluoro-chloro triaryl-boranes and amines within the same reaction.



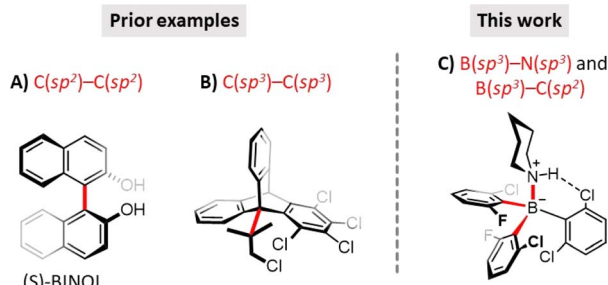


Fig. 1 Selected examples of molecules featuring (A)  $C(sp^2)-C(sp^2)$  and (B)  $C(sp^3)-C(sp^3)$  atropisomeric states<sup>10</sup> and a (C) dual  $B(sp^3)-N(sp^3)$  and  $B(sp^3)-Ar(sp^2)$  type atropisomeric adducts reported in our present work. Bonds corresponding to restricted rotations are highlighted in red.

The challenge outlined inevitably poses an additional fundamental question: when do we consider configurational, conformational, and stereochemical isomers as distinct, isomeric molecules with different properties, including reactivity and symmetry? This question cannot be answered without specifying important experimental conditions such as the time scale of observation, temperature, pressure, *etc.* That is, these molecular properties are definable only within limits. As an example, owing to the sterical congestion, *R*- and *S*-binaphthol (Fig. 1A) are atropisomers at ambient temperature and fundamental chiral building blocks for chiral catalysis. So, these conformational isomers are distinct molecules at room temperature with different reactivities in asymmetric reactions. Nevertheless, over 200 °C reaction temperature or million years of observation period, *R*- and *S*-binaphthols should be treated as non-distinct, equivalent molecules.

In virtue of above, we had to specify the external parameters under which the existence of MLA was investigated. Considering practical aspects and the potential of future use, we have confined ourselves to the most relevant parameters of routine organic chemistry (*e.g.* ambient temperature, 1 atm pressure, and ms-days timescale). Thus, to be distinguished as distinct molecules, the formed isomeric dative LA-LB adducts must be detectable by NMR at ambient temperature. Additionally, the structure of the LA should be such that its conformational isomers can be handled as non-distinct, equivalent molecules at ambient temperature. So, the sterical congestion around the Lewis acidic center must be large enough to form atropisomeric dative adducts, but not too large to halt the conformational isomerism of the LA itself at ambient temperature.

It is then worthwhile to further specify the phenomenon of single-centered, but multiple Lewis acidity and to discuss the challenges associated with its observation. First and foremost, the presence of non-equivalent, diastereotopic faces as distinct 'binding sites' of the Lewis acid is a necessary but not sufficient condition for MLA. It is possible that, for steric and/or electronic reasons, only one dative adduct is produced, *i.e.* a diastereoselective adduct formation occurs and single Lewis acidity can be determined (Fig. 2A).<sup>9a,e</sup> If the formation of multiple adducts is kinetically and thermodynamically possible, we

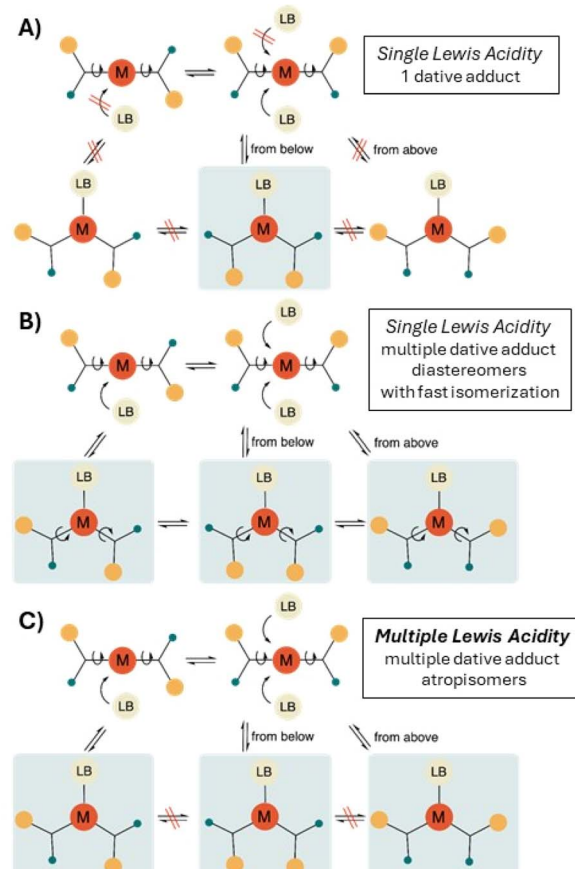


Fig. 2 The distinction between single Lewis acidity and multiple Lewis acidity (MLA) among diastereotopic Lewis acids. (A) The diastereotopic LA shows a single Lewis acidity due to diastereoselective adduct formation towards a LB. (B) There is no diastereoselectivity upon dative adduct formation but if the thermodynamic equilibrium between the detected LA-LB adducts is established by rapid conformational isomerisation and slow dissociation-association, then the situation should be considered a case of single Lewis acidity. (C) In the clear-cut, straightforward form of MLA, the distinct atropisomeric conformational states of the dative adduct are all formed in separate reactions and can only interconvert via the breaking and reforming of the dative bond.

might expect that all observable atropisomeric dative adducts are formed in different, mutually competitive chemical reactions between the same LA and LB. However, if the thermodynamic equilibrium between the detected LA-LB adducts is also established by rapid conformational isomerisation (*via* rotation around single bonds) as well as slow dissociation-association, then the situation should be considered a case of single Lewis acidity, which, again, can be described by a single equilibrium constant (Fig. 2B). Thus, multiple Lewis acidity can only emerge, if either stable, non-dissociable atropisomeric dative adducts are formed between the diastereotopic LA and the same LB (in a kinetically controlled manner) or the interconversion of the atropisomeric dative adducts requires the breaking and reforming of the dative bond (Fig. 2C). Indeed, in the latter case each LA-LB atropisomer represents a reversible association pathway, and thus, the Lewis acidity can be described by as



many equilibrium constants as the number of LA–LB atropisomer detected. Finally, it should be noted that not only the strength of Lewis acidity (hydricity, Gutmann–Beckett, *etc.*), but also its multiplicity is a situation-dependent phenomenon, so it can happen that the very same LA can exhibit single or multiple Lewis acidity with different LBs.

In this paper, we report chemical evidence that the hypothesized phenomenon that enables multiple Lewis acidity to be assigned exists, even at ambient temperature. Indeed, combined computational and NMR studies revealed that the crowded LA–LB atropisomeric adducts (Fig. 1C) display such high rotational barriers that their isomerization pathway is dissociative.

## Results and discussion

### Diastereotopicity of non-symmetrically halogenated triarylboranes

To encounter single-centered MLA and characterize the corresponding atropisomers, we turned our focus towards frustrated Lewis pair<sup>11</sup> (FLP) chemistry. This field employs specific LA and LB combinations that are incapable of stable dative adduct formation due to steric hindrance. Thus, a ‘quasi-metastable’ state arises that can be utilized for bond activation in multiple reactions including hydrogenation.<sup>12</sup> Recently, we developed a set of halogenated triaryl-borane catalysts for FLP promoted reductive aminations.<sup>13</sup> To optimize catalyst performance, we deliberately replaced the F atoms in *ortho* positions with Cl

atoms that provided a set of fluoro-chloro boranes, **I**, **II** and **III** (Fig. 3A) with gradual differences both in their steric and electronic properties. Since the metrics of Lewis acidity are base-dependent, various complementary methods have been used to assess their LA strength, corresponding to global, effective and intrinsic Lewis acidity.<sup>14</sup> As expected for such sterically crowded systems, there has been an offset between these complementary methods. Surprisingly, however, these methods and catalytic test reactions indicated a non-linear relationship between the level of F-to-Cl substitution and the relative Lewis acidity (especially the Gutmann–Beckett method<sup>15</sup>) or the catalytic activity.<sup>13</sup> Indeed, while the introduction of the bulkier Cl atoms into boranes **II** and **III** gradually increased the electron deficiency of the boron centers, it profoundly reshaped the energy landscape of their dative adducts with  $\text{Et}_3\text{P}=\text{O}$  or the hydride anion ( $\text{H}^-$ ) through the counteracting change in steric effects (front- and back-strains).

This interesting and somewhat unusual behavior upon dative adduct formation prompted us to conduct further and more detailed structural studies with boranes **I**–**III**. After a thorough analysis of their structures, we postulated that each of these special boranes individually features diastereotopic faces (Fig. 3), possibly resulting in diastereomeric adducts upon interaction with an achiral LB and thus might possess MLA. In these  $\text{BAr}_3$  structures, the aryl rings adopt propeller shaped conformations (see the computed **I**–**III** rotameric states in ESI Section 2 in the ESI†); however, the particular *o*-F and *o*-Cl substitution patterns decrease the molecular symmetry and

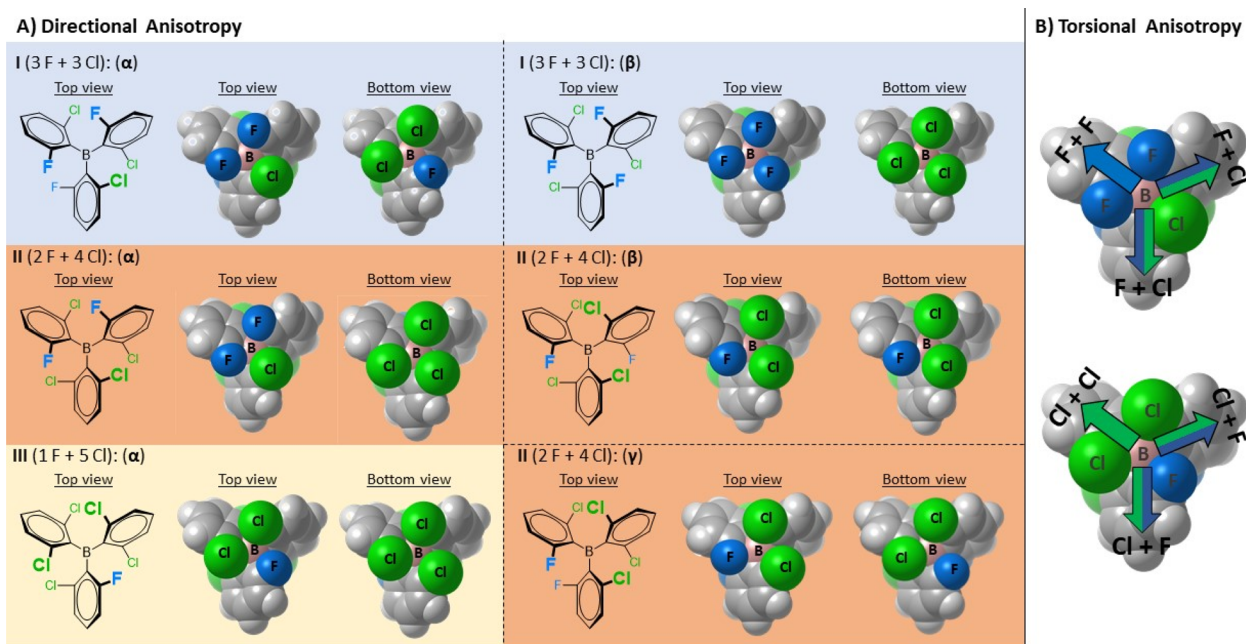


Fig. 3 (A) Illustration of the diastereotopicity of non-symmetrically halogenated triaryl-borane catalysts **I**, **II** and **III** (highlighted with blue, orange and cream backgrounds). Due to the presence of only one non-symmetrically substituted aryl ring, borane **III** has only one rotamer. The rotameric states of each borane are shown in van der Waals representations from top and bottom views. The corresponding rotameric states are denoted with Greek letters which refer to the order of their calculated stability, with the  $\alpha$ -state being the respective lowest energy state (Table S2†). (B) Illustration of the torsional anisotropy upon dative bond formation with appropriate Lewis bases (having no  $\text{C}_3$  symmetry) using the top and bottom views of the **I**( $\alpha$ ) structure. The colored arrows indicate distinct molecular confinements for the incoming Lewis base. The F atoms are colored blue, and the Cl atoms are colored green.



these boranes can display both directional and torsional structural anisotropy upon dative adduct formation. In contrast to **III**, a more complex situation is expected to emerge for boranes **I** and **II**, as the rotation of the non-symmetrically substituted aryl rings around the  $B(sp^2)$ -Ar( $sp^2$ ) single bonds results in multiple rotamers (2 and 3 for **I** and **II**, respectively), which, in principle, would further diversify the global and intrinsic Lewis acidities and their diastereotopicity. Additionally, we also hypothesized that the distinct conformations of the dative borane adducts might be detected as the enhanced rotational barriers imposed upon the dative adduct formation would hinder the rotational isomerism of the thermally accessible conformational states. Accordingly, these isomeric LA-LB adducts would be atropisomers, stemming from directional and/or torsional anisotropy of the LA upon dative bond formation and the hindered internal rotations around the  $B(sp^3)$ -Ar( $sp^2$ ) and  $B(sp^3)$ -N( $sp^3$ ) single bonds (using N-based LB).

### Computed hydride-borane adduct atropisomers

Having dissected the stereochemical features of boranes **I-III**, we addressed the question whether their atropisomeric dative adducts are sufficiently populated at ambient temperature, thereby not imposing constraints on detecting the MLA phenomenon, *i.e.* the Fig. 2A case. The selected hydride anion LB was expected to scan the diastereotopicity of the borane rotamers without the complicating effects of torsional anisotropy and front strain (Fig. 4). Thus, we carried out quantum chemical calculations to determine the thermodynamic driving force ( $\Delta G^h$ ) to generate the  $[H-I]^-$ ,  $[H-II]^-$  and  $[H-III]^-$  hydride dative adducts of distinct conformational states. The geometry optimizations and the estimation of finite temperature and

solvent effects were carried out at the B3LYP-D3/6-311G(d,p) level of DFT. For relative stability predictions, the electronic energies were computed for the optimized geometries using the LNO-CCSD(T) method extrapolated to the complete basis set (CBS) limit (for additional computational details, see the ESI†). Most importantly, as displayed in Fig. 4, for each of **I**,<sup>16</sup> **II** and **III** the MLA phenomenon can in principle be a possibility as even the less stable conformers of their respective hydride adducts are predicted to be sufficiently populated ( $\Delta\Delta G^h \leq 3.5$  kcal mol<sup>-1</sup>). Namely, there is no thermodynamic driving force for diastereoselective hydride adduct formation. Nevertheless, potential energy scan analysis (ESI Section 8†) indicated that the  $B(sp^3)$ -Ar( $sp^2$ ) bonds can freely rotate in these hydride adducts, suggesting that these are still single Lewis acidity cases, *i.e.* the Fig. 2B case, and their Lewis acidity, paired with the hydride anion LB (hydricity), should be calculated as a population weighted average of all the different conformers/atropisomers. Notably, for any borane studied, the rotameric state with the most fluorine atoms on the side opposite to the attacking hydride yields the most stable hydride adduct as it imposes the weakest back-strain effects (see strain-analysis in ESI Section 11†).

### Detection of the piperidine-borane adducts' atropisomeric states

Next, we sought to identify a suitable LB which can evoke the case of multiple Lewis acidity in the dative adduct formation with boranes **I**, **II** and **III**. Importantly, the <sup>19</sup>F NMR spectra of the respective boranes (Fig. S9-S11†) showed an averaged <sup>19</sup>F signal indicating that there were no distinct rotamers in the  $sp^2$  state at ambient temperatures due to the free rotation around the boron center. To investigate not only the structural but also

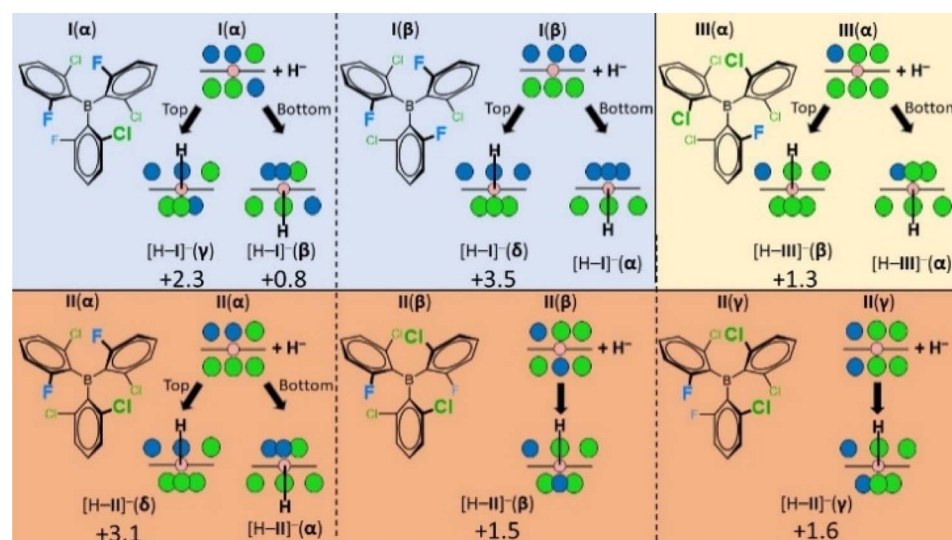


Fig. 4 The schematic representation of the triaryl-borane structures and their hydride adducts (F: blue, Cl: green, and B: pink spheres). The 'top' and 'bottom' approaches refer to the diastereotopic views presented in Fig. 3. In the  $sp^3$  states the spatial density of halogen ligands differs on the two sides of the adducts leading to increased back-strain (congested ligands) and decreased front-strain (sparser ligands). The combination of rotameric states and diastereotopic faces engenders multiple, atropisomeric hydride adduct conformers for each borane. The respective  $\Delta G^h$  values are shown in Table S3.† Here, the  $\Delta\Delta G^h$  values with respect to the most stable conformational state ( $\alpha$ ) are indicated for the higher energy hydride adduct conformers in kcal mol<sup>-1</sup> at 298.15 K.



the dynamic properties of the emerging dative adducts of these boranes, various NMR methods and complementary computational studies were utilized. Although detection of conformational isomers of small molecules is inherently challenging using ensemble methods such as NMR spectroscopy, screening of a variety of commercially available amines proved successful. Indeed, in most cases, either the lack of dative adduct formation or rapid isomerization in the  $sp^3$  state could be detected (for details on the full library of LB amines see ESI Fig. S2 $\dagger$ ) providing no clear-cut proof for the MLA phenomenon (Fig. 2B). Gratifyingly, piperidine (**p**) was found to be able to form atropisomeric, long-lived dative adducts with each of **I**, **II**, and **III**, demonstrated by  $^{19}F$  NMR (for all  $^{19}F$  NMR spectra see ESI Section 3 $\dagger$ ). Exemplified by the  $^{19}F$  NMR spectra of the **p** + **II** mixture, in the slow exchange regime (Fig. 5) the  $^{19}F$  signals of the distinct **p**-adduct atropisomers are well-resolved and appear typically high upfield- ( $<-107$  ppm) or downfield-shifted ( $>-90$  ppm) with respect to the non-interacting  $sp^2$ -hybridized borane **II** signal ( $\sim-100$  ppm, see Fig. S12–S14 $\dagger$ ). Importantly, **p** is a structurally more complex and sterically more demanding LB than the  $H^-$  and is suitable to probe the torsional anisotropy (Fig. 3B) of boranes **I–III** as well. Thus, upon the approach of **p** to a particular diastereotopic face of **I**, **II** or **III**, even more dative-adduct atropisomers might emerge due to the rotational constraints around the  $B(sp^3)-N(sp^3)$  dative bond. Indeed, for all three boranes, the number of the corresponding **p**-adduct  $^{19}F$  signals is always a multiple of the number of F atom(s) in the given borane, which implies that the adducts **p–I**, **p–II** and **p–III**

present several stable atropisomeric states simultaneously. Also notable is that after adding 3 equivalents of **p**, the  $^{19}F$  signal of the  $sp^2$ -hybridized boranes was not observable in the spectra of **I** and **II** and they remained absent even at higher temperatures. In contrast, the free borane **III** was still observable in the slow exchange regime owing to its highly crowded structure; thus, its ‘free’  $sp^2$  state with **p** is preferred. The dative bond formation between **p** and the boranes and the concomitant changes in electron density around the boron atom were further corroborated by  $^{11}B$  NMR (for the  $^{11}B$  spectra, see Fig. S3–S8 $\dagger$ ).

To aid the structural assignment of the expected atropisomeric states of **p–I**, **p–II** and **p–III**, computational studies were conducted (ESI Section 4 $\dagger$ ) following the structure calculation protocol used for the hydride adduct calculations (all computed **p**-borane structures along with the corresponding  $\Delta G^a$  values are reported in Tables S4–S6 $\dagger$ ). Importantly, the calculated dative **p**-adduct structures display clear differences from the hydride adducts as a result of enhanced steric effects and the lower symmetry of the **p** LB. Nevertheless, they share a common molecular topology regarding the relative orientation of **p** and the borane’s aryl rings. This is illustrated in Fig. 6A with the energetically lowest lying ( $\alpha$ ) conformer of **p–II**. The structurally common features are (i) the N atom of **p** donates the equatorial lone electron pair to the boron to establish the dative bond, (ii) one borane’ aryl ring is oriented vertically thereby pointing one of its halogen atoms towards the amine proton of **p** ( $H^N$ ) to form a hydrogen bond, and (iii) the second borane’ aryl ring, which also interacts with  $H^N$ , is tilted about  $45^\circ$  from the B–N axis (iv)

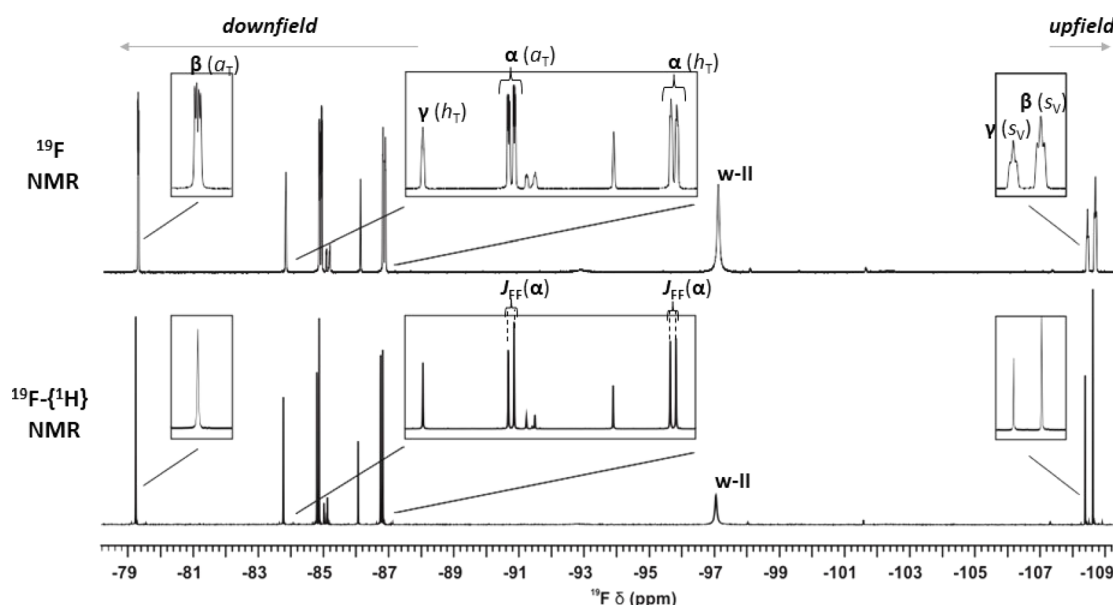


Fig. 5 The 1D  $^{19}F$  NMR spectrum (564 MHz, 298.2 K) of a mixture of **p** and **II** in toluene-d8 using a **p** to **II** ratio of 3 : 1 without (top) and with (bottom)  $^1H$ -decoupling during acquisition. The two F atoms in **p–II** combined with the three distinct atropisomeric states ( $\alpha$ ,  $\beta$ , or  $\gamma$ ) generate six resolved **p–II**  $^{19}F$  signals. The represented conformation and specific F atom position ( $a_V$ ,  $a_T$ ,  $h_V$ ,  $h_T$ ,  $s_V$  or  $s_T$ , see Fig. 6A) are indicated for each **p–II** signal. For the **p–II**( $\alpha$ ) signals the effect of  $^{19}F$ – $^{19}F$  through a space  $J$ -coupling ( $J_{FF}$ ) of 39.5 Hz between the  $a_T$  and  $h_T$  positioned  $^{19}F$  spins is apparent as in the  $^1H$ -decoupled spectrum they remain doublets as opposed to the **p–II**( $\beta$ ) and **p–II**( $\gamma$ ) signals which simplify to a singlet. The broad signal marked as ‘w-II’ that remains close to the  $sp^2$ -hybridized borane peak position represents slowly diffusing species that comprise interacting **II**, **p**, and residual water molecules encompassed in a single solvent cage (the characterization of these aqueous species is detailed in ESI Section 9 $\dagger$ ).



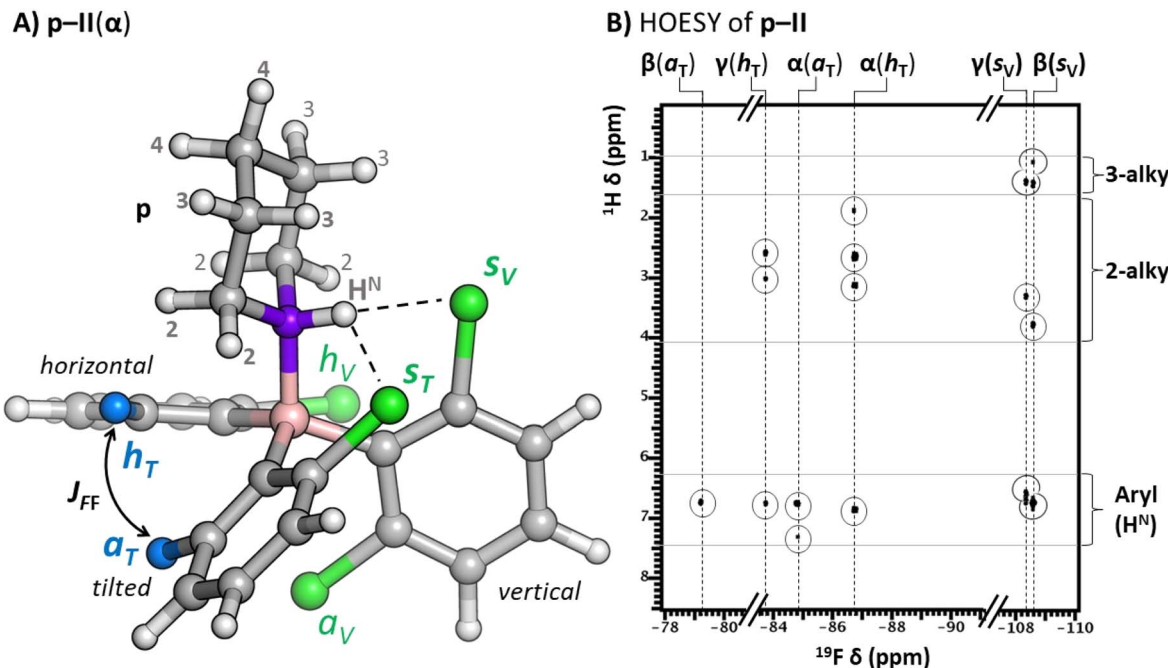


Fig. 6 (A) The common ring topology of the computed **p**-adduct structures illustrated with the lowest lying ( $\alpha$ ) conformation of **p**-II. The emerging halogen atom positions are denoted as horizontal (*h*), *syn* (*s*) or *anti* (*a*) whereas the subscripts specify whether the halogen atom is located on (*s*, *a*) or points towards (*h*) the tilted (*T*) or vertical (*V*) ring. The hydrogen bonding interaction between the  $\text{H}^{\text{N}}$  and the *syn*-positioned ligands is indicated with black dashed lines. The **p**-II( $\alpha$ ) features the two F atoms (blue) in the  $\alpha_{\text{T}}$  and  $h_{\text{T}}$  positions through which a through-space  $J_{\text{FF}}$  coupling of 39.5 Hz emerges (see  $\alpha(\alpha_{\text{T}})$  and  $\alpha(h_{\text{T}})$  signals in Fig. 5). (B) The  $^{19}\text{F}$ - $^1\text{H}$  HOESY correlations of the **p**-II atropisomers ( $\alpha$ ,  $\beta$  and  $\gamma$ ) are highlighted with circles. The *s*-fluorines (of the  $\beta$  and  $\gamma$  atropisomers) are found sufficiently close in space to most of the **p** ring to be correlated with the  $\text{H}^{\text{N}}$  and most of the alkyl **p** hydrogens; the *h*-fluorines ( $\alpha$ ,  $\gamma$ ) are correlated with a limited number of alkyl **p** hydrogens; in contrast, the *a*-fluorines ( $\alpha$  and  $\beta$ ) do not display HOESY contacts with **p**.

while the third aromatic ring is in horizontal orientation, that is, nearly perpendicular to the B-N axis. We designated the emerging halogen atom positions on the vertical and tilted aryl rings as being in the ‘*syn*’ or ‘*anti*’ position with respect to the incoming **p**. Thus, given the observed ring topology preference, any **p**-adduct atropisomer can be defined in a straightforward way through the specific F/Cl spatial distribution pattern between the *horizontal* (*h*), *syn* (*s*) and *anti* (*a*) position pairs. Notably, due to the emerging hydrogen bond with the *syn* positioned aryl halides and back-strain interactions, in all three **p**-borane systems, the vertical and tilted fluorinated ring(s) prefer the F atom in the *syn* and *anti* positions, respectively. Also, the horizontal fluorinated ring adopts a more stable orientation with the F atom pointing towards the tilted ring. Based on the computed Gibbs free energies of adduct formation ( $\Delta G^{\text{a}}$ ) the expected affinity of the boranes for dative bonding with **p** follows the general order of **III** < **II** < **I** which indicates the impact of the growing back-strain to destabilize the dative adducts (Tables S4–S6<sup>†</sup>). The importance of back-strain effects in adduct formation is supported by activation-strain analysis presented in ESI Section 11.<sup>†</sup> We also note that the presence of hydrogen bonds in these piperidine-borane adducts may contribute considerably to the thermodynamic stability of the various atropisomeric adducts (although the most stable isomers feature the weaker Cl···H-N bond), but it is unlikely that the hydrogen bonding interactions (acting as a ‘structural pin’<sup>17</sup>) are the prerequisite of the formation of distinguishable

atropisomeric states. This is confirmed by the fact that borane-LB adducts formed with bases having no N-H protons (for instance LB = quinuclidine, see Section 12 of the ESI<sup>†</sup>) also show multiple resonances in the  $^{19}\text{F}$  NMR spectra, pointing to multiple atropisomeric adduct states.

To validate the assignment of the experimentally observed **p**-borane atropisomeric states to the computed structures,  $^{19}\text{F}$  chemical shift calculations (ESI Section 5<sup>†</sup>) at the B3LYP-D3/6-311+G(2d,p) level of DFT and  $^{19}\text{F}$ - $^1\text{H}$  HOESY<sup>18</sup> measurements (Fig. 6B, S28 and S29<sup>†</sup>) were performed. These revealed correlations in the frequency, linewidth, and fine structure of the  $^{19}\text{F}$  signals with the fluorine atom allocated to the proposed *horizontal*, *syn* or *anti* position (for the full  $^{19}\text{F}$  NMR signal assignment process see ESI Section 6<sup>†</sup>). That is, the hydrogen bonding interaction of *syn* positioned fluorines with the **p** N-H group is

Table 1 Fluorine atom positions in the detected atropisomeric states per **p**-borane adduct. The respective atropisomeric states are denoted with Greek letters according to their experimental distribution probability (indicated in parenthesis) obtained from  $^{19}\text{F}$  NMR signal integrals

<b>p</b> -Borane adduct	Detected atropisomer			
	$\alpha$	$\beta$	$\gamma$	$\delta$
<b>p</b> -I	$a_{\text{T}} s_{\text{V}} h_{\text{T}}$ (85%)	$a_{\text{T}} a_{\text{V}} h_{\text{T}}$ (10%)	$a_{\text{T}} s_{\text{V}} h_{\text{V}}$ (3%)	$s_{\text{V}} s_{\text{T}} h_{\text{T}}$ (2%)
<b>p</b> -II	$a_{\text{T}} h_{\text{T}}$ (51%)	$a_{\text{T}} s_{\text{V}}$ (30%)	$h_{\text{T}} s_{\text{V}}$ (19%)	
<b>p</b> -III	$a_{\text{T}}$ (61%)	$h_{\text{T}}$ (30%)	$s_{\text{V}}$ (9%)	

reflected by the upfield shift of their  $^{19}\text{F}$  signals and the unusually high  $^1\text{H}$ – $^{19}\text{F}$   $J$ -coupling of 20–25 Hz that exists through the  $\text{H}\cdots\text{F}$  hydrogen bond.<sup>19</sup> By distinguishing the downfield-shifted *horizontal* and *anti*-positioned  $^{19}\text{F}$  signals as well, we concluded that the respective 4, 3 and 3 computed atropisomeric states of **p-I**, **p-II** and **p-III** indeed form under experimental conditions (Table 1). Our assignment was further supported by the good agreement between the experimental and computed  $^{19}\text{F}$  chemical shifts (Fig. S30†) and conformational probability distributions (Table S10†). The spatial vicinity of fluorine atoms in the **p-I**( $\alpha$ ), **p-I**( $\beta$ ), **p-I**( $\delta$ ) and **p-II**( $\alpha$ ) structures could be confirmed by  $^{19}\text{F}$ – $^{19}\text{F}$  through space  $J$ -couplings<sup>20</sup> ( $J_{\text{FF}}$ ) ranging between 15 Hz and 80 Hz (all the extracted  $J_{\text{FF}}$  values are specified in Table S9†).

### Kinetic stability of the piperidine-borane adducts

At room temperature, due to the kinetic lability of the dative **p-III** adduct, the  $\text{sp}^2$  **III** and the **p-III** atropisomeric states are not detectable as they are in fast exchange at the NMR timescale (Fig. S15†). In contrast, for the **p + II** and **p + I** systems the respective  $\text{sp}^2$  state and dative adduct atropisomer signals are resolved (**p + II**: *e.g.* Fig. 5 or S16†; **p + I**: *e.g.* Fig. S17†). Notably, for the **p + II** and **p + I** systems applying the piperidine : borane = 1:1 ratio or excess of piperidine, the  $\text{sp}^2$  borane signal remains unobservable due to the high conversion rate of piperidine and the boranes into the corresponding dative adducts. Thus, to detect the  $\text{sp}^2$  signal, excess of the borane is required.

Further insights into the kinetic stability of the observed **p**-adducts were also gained through the temperature dependence of the linewidths in the corresponding  $^{19}\text{F}$ -NMR spectra. The

NMR peaks of **p-III** resolve at low temperatures (<253 K) only; however, they display severe line broadenings throughout (Fig. S15†). At ~273 K, the signals start to coalesce, and at higher temperatures a weighted average signal is visible that represents the fast-exchanging ensemble of the **p-III** atropisomers and the borane **III** (which notably incorporates the ‘frustrated’ state). The signals of **p-II** display moderate line broadenings starting at 293 K and they remain in the slow exchange regime even at 333 K (Fig. S16†); while the signals of **p-I** do not display any broadenings unless the temperature is raised to 323 K (Fig. S17†). These results imply that the kinetic stability of the **p**-adducts follows the order of **III** < **II** < **I** which is in agreement with the thermodynamic trend predicted by computation.

### Dynamic behavior of the piperidine-borane atropisomeric adducts

After observing the existence of multiple distinct atropisomeric LA-LB adducts at ambient temperature, we started to investigate their dynamic behavior in order to verify if the MLA can be assigned to these systems. To characterize the emerging dynamic behavior of the dative piperidine–borane adducts, two-dimensional  $^{19}\text{F}$  Exchange Spectroscopy (EXSY) measurements<sup>21</sup> were performed in the slow exchange regime (for all the EXSY spectra, the extracted exchange rate constants and thermodynamic parameters see ESI Section 7.†) To retain the  $\text{sp}^2$ -hybridized borane state observable throughout, the **p**:borane ratio was inverted to 1:2 in the mixtures of **p** with **I** or **II**. Under optimal experimental conditions (temperature, mixing time) the corresponding 2D  $^{19}\text{F}$  EXSY spectra show qualitatively the same behavior for all the **p**-adducts, *see that of the **p + II** system as illustrated in Fig. 7 (**p + III**: ESI Fig. S31, **p + I**: Fig. S33†)*. That

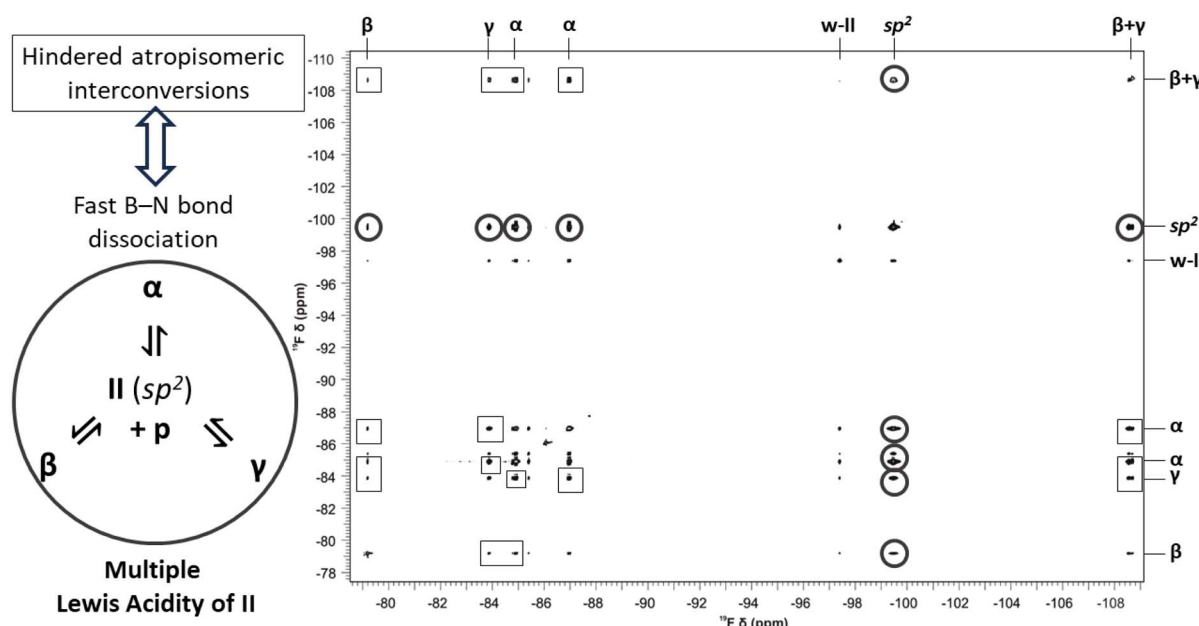


Fig. 7 The  $^{19}\text{F}$ -EXSY spectrum (564 MHz) of the **p + II** system using a **p** to **II** ratio of 1:2. The spectrum was recorded at 333.0 K with a mixing time of 33 ms. The  $^{19}\text{F}$  frequencies are assigned along both dimensions with the distinct **p-II** atropisomer signals indicated with Greek letters. Cross-peaks indicating the fast exchanges that involve the  $\text{sp}^2$  **II** form and the dative **p-II** atropisomers are highlighted with circles. The hindered exchanges taking place between the atropisomers of **p-II** are highlighted with squares.



is, each fluorine resonance of any chosen **p**-adduct atropisomer shows correlation peaks with those of its other atropisomers and with the corresponding  $sp^2$  form as well. These respectively indicate that on the timescale of the experiments the simultaneously existing **p**-adduct atropisomeric states are in slow exchange with each other; meanwhile, they undergo rapid dissociation and reassociation of the B–N dative bond through the dissociated states of the atropisomeric adduct. The exchange processes and the related barriers are illustrated in Fig. 8 in terms of schematic free energy surface projections. Based on the corresponding conformational exchange rates and dissociation rates (**p**-**I**: Table S16, **p**-**II**: Table S13, and **p**-**III**: Table S11†) extracted from the EXSY peak integrals (ESI Section 1.1†), for any given atropisomeric state of **p**-**I** or **p**-**III** its exchange with another atropisomer is generally 1–2 orders of magnitude slower than its dissociation. Unfortunately, signal overlaps prevented us from unequivocally quantifying the exchange rates for **p**-**II** with the free borane **II** (Fig. S10†). Nevertheless, a 2D  $^{19}\text{F}$  EXSY spectrum was recorded on the **p**-**II** system with minimal mixing time (2 ms) that displays the exchanges of **p**-**II** with the free borane **II** while the atropisomeric exchanges remain unobservable (Fig. S32†). Furthermore, for **p**-**I** and **p**-**II** the atropisomeric exchanges appear to be parallel in terms of fluorine NMR exchanges, that is, any F atom of a detected atropisomer undergoes chemical exchanges with all the F atoms of each detected atropisomer. The exchange rates of the different F-pairs that can be associated with the same atropisomeric exchange fall within an order of magnitude (Table S12†). Consequentially, upon an atropisomeric exchange process there is no correlation between the initial and final position of the F atoms, that is, the orientation of the aryl rings. All these imply that, for the atropisomeric exchanges of these **p**-borane adducts, neither free nor correlated rotation<sup>22</sup> around  $\text{B}(\text{sp}^3)\text{–Ar}(\text{sp}^2)$  or  $\text{B}(\text{sp}^3)\text{–N}(\text{sp}^3)$  single bonds of the dative adduct is operative. Thus, the atropisomeric exchanges for the investigated **p**-adducts, *i.e.* their conformational isomerism rather take place through the  $sp^2$  borane state where the rotations of the aryl rings are free and essentially, they occur as the side-processes of the dissociation–reassociation equilibrium between **p** and the borane (Fig. 8). Accordingly, all **p**-borane atropisomers are formed in different chemical reactions

between the same Lewis acid (**I**, **II** or **III**) and base (**p**) which directly proves the concept of MLA for these triaryl-boranes. To further corroborate this finding, a series of DFT potential energy surface scans were performed using the **p**-**II**( $\alpha$ ) and **II** structures (ESI Section 8†). These showed that in contrast with the  $sp^2$  borane state (12–14 kcal mol<sup>−1</sup>), rotations around the central  $\text{B}(\text{sp}^3)$  atom (*i.e.* B–C and B–N bonds) are hampered in the dative bonded **p**-adduct state with the associated barrier heights ranging between 25 and 53 kcal mol<sup>−1</sup>. These values are also significantly higher than the experimentally measured barrier heights (17–20 kcal mol<sup>−1</sup>) for the atropisomeric exchanges of the **p**-**II** adduct (Table S14†) which denote the interconversion of the **p**-adduct atropisomeric states *via* internal rotations in comparison to the breaking of the dative B–N bond. Hence, in the case of these dative adducts, the non-stable dative bonding underlies the conformational dynamic equilibrium between their respective atropisomers *via* breaking and reforming the dative bond and it seems that these atropisomers have a rather rigid structure, ultimately adhering to the nomenclature ‘atropos’, *i.e.* ‘without turn’.

## Conclusions

In summary, we demonstrated the emergence of a noteworthy molecular phenomenon, the single-centered, but multiple Lewis acidity for specific Lewis acidic boranes. The observation of this particular property was possible for ortho-halogenated triaryl-boranes, **I**, **II** and **III**, with appropriate steric crowding and symmetry design around the Lewis acidic center. These boranes proved to be able to form atropisomeric and kinetically labile dative adducts with piperidine owing to their inherent structural anisotropy and hindered internal rotation in the LA–LB adducts around the  $\text{B}(\text{sp}^3)\text{–Ar}(\text{sp}^2)$  and  $\text{B}(\text{sp}^3)\text{–N}(\text{sp}^3)$  bonds. The static and dynamic properties of the atropisomeric, dative piperidine-borane adduct ensembles were investigated by NMR spectroscopy and computational structural analysis. Notably, the evolving back strain upon dative adduct formation influenced not only the thermodynamics but also the kinetics of the dissociative equilibria in which the atropisomeric interconversions are fundamentally dissociative in nature as they take place *via* the ‘frustrated’ or the entirely dissociated state of the  $sp^2$  borane. In addition to revealing a non-conventional molecular phenomenon *via* elusive dative adduct atropisomers, these findings are expected to broaden the current conceptual framework of Lewis acidity and draw attention to the possible emergence of a more complex scenario upon Lewis acidity strength assessment. Additionally, our work provides a tool that is ready to be placed at the disposal of chemists to evoke this property and may open new vistas for the deliberate design of diastereomeric assemblies in materials and biological science<sup>23</sup> and development of homogeneous confined catalysts with built-in functionality or higher-order stereogenicity.<sup>24</sup>

## Data availability

The data that supports the findings of this study are available in the ESI of this article.†

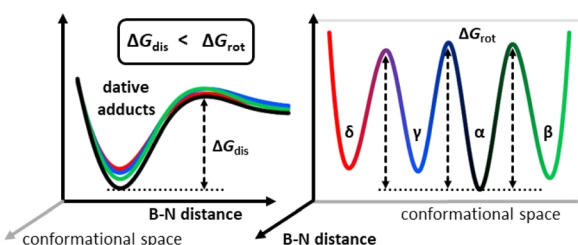


Fig. 8 Schematic illustration of free energy surfaces of the atropisomeric states and the dissociation pathways of **p**-borane adducts. Various atropisomers are denoted by Greek letters and color codes. The dissociation is represented by the B–N distance as a reaction coordinate (left), and the conformational *via* rotations around the  $\text{B}(\text{sp}^3)\text{–N}(\text{sp}^3)$  and  $\text{B}(\text{sp}^3)\text{–C}(\text{sp}^2)$  bonds in the adduct states are illustrated along the conformational space coordinate (right).

## Author contributions

B. Kovács assigned the p-borane adduct atropisomers and created the original drafts of the manuscript together with T. S. and T. F. The NMR measurements were performed by M. S., and B. Kovács and A. D. M. S. obtained the kinetic and thermodynamic data of the p-borane adducts. The computations were designed and analyzed by T. F. with the contribution of B. Kótai and G. L. under the supervision of I. P. The X-ray structures were determined by T. H. É. D. synthesized the boranes and prepared the NMR samples. The concept of multiple Lewis acidity was conceived by T. S. All authors have given approval to the final version of the manuscript.

## Conflicts of interest

There are no conflicts to declare.

## Acknowledgements

Financial support from the National Research, Development, and Innovation Office (NKFIH) is gratefully acknowledged (grants K-142486, K-147280 and ÚNKP-23-3-I-ELTE-206). We greatly appreciate the referees' insightful and helpful comments on our manuscript, which improved its quality and clarity.

## Notes and references

- 1 Selected reviews: (a) R. W. Hoffmann, *Angew. Chem., Int. Ed.*, 1992, **31**(9), 1124–1134; (b) S. D. Appavoo, S. Huh, D. B. Diaz and A. K. Yudin, *Chem. Rev.*, 2019, **119**(17), 9724–9752; (c) H. K. Ganguly and G. Basu, *Biophys. Rev.*, 2020, **12**(1), 25–39.
- 2 Recent studies focusing on conformers: (a) G. C. A. da Hora, M. Oh, M. C. Mifflin, L. Digal, A. G. Roberts and J. M. J. Swanson, *J. Am. Chem. Soc.*, 2024, **146**(7), 4444–4454; (b) S. H. Rüdisser, E. Matabaro, L. Sonderegger, P. Güntert, M. Künzler and A. D. Gossert, *J. Am. Chem. Soc.*, 2023, **145**(50), 27601–27615; (c) R. K. R. Sannapureddi, M. K. Mohanty, L. Salmon and B. Sathyamoorthy, *J. Am. Chem. Soc.*, 2023, **145**(28), 15370–15380; (d) X. Fu, B. Zhu and X. Hu, *J. Am. Chem. Soc.*, 2023, **145**(29), 15668–15673; (e) E. B. Crull, A. N. Jain, P. C. D. Hawkins, A. E. Cleves, E. I. Graziani and R. T. Williamson, *J. Nat. Prod.*, 2023, **86**(7), 1862–1869; (f) C. M. Nunes, J. P. L. Roque, S. Doddipatla, S. A. Wood, R. J. McMahon and R. Fausto, *J. Am. Chem. Soc.*, 2022, **144**(45), 20866–20874; (g) F. Bohle and S. Grimme, *Angew. Chem., Int. Ed.*, 2022, **61**(14), e202113905; (h) B. Linclau, Z. Wang, B. Jeffries, J. Graton, R. J. Carbo, D. Sinnaeve, J.-Y. Le Questel, J. S. Scott and E. Chiarparin, *Angew. Chem., Int. Ed.*, 2022, **134**(7), e202114862; (i) R. Costil, A. J. Sterling, F. Duarte and J. Clayden, *Angew. Chem., Int. Ed.*, 2020, **59**(42), 18768–18773; (j) P. J. Canfield, I. M. Blake, Z.-L. Cai, I. J. Luck, E. Krausz, R. Kobayashi, J. R. Reimers and M. J. A. Crossley, *Nat. Chem.*, 2018, **10**(6), 615–624.
- 3 Selected examples: (a) K. Iizuka, H. Takezawa and M. Fujita, *J. Am. Chem. Soc.*, 2023, **145**(48), 25971–25975; (b) R. E. Looper, D. Pizzirani and S. L. Schreiber, *Org. Lett.*, 2006, **8**(10), 2063–2066; (c) M. Kindermann, I. Stahl, M. Reimold, W. M. Pankau and G. von Kiedrowski, *Angew. Chem., Int. Ed.*, 2005, **117**(41), 6908–6913; (d) H. Yamataka, O. Aleksiuk, S. E. Biali and Z. Rappoport, *J. Am. Chem. Soc.*, 1996, **118**(50), 12580–12587; (e) R. S. Brown, H. Slebocka-Tilk, A. J. Bennet, G. Bellucci, R. Bianchini and R. Ambrosetti, *J. Am. Chem. Soc.*, 1990, **112**(17), 6310–6316; (f) Z. Rappoport and S. E. Biali, *Acc. Chem. Res.*, 1988, **21**(12), 442–449; (g) T. T. Tidwell, *Tetrahedron*, 1978, **34**(13), 1855–1868; (h) S. Milstien and L. A. Cohen, *Proc. Natl. Acad. Sci. U.S.A.*, 1970, **67**(3), 1143–1147; (i) T. Hannah and S. S. Chitnish, *Chem. Soc. Rev.*, 2024, **53**(2), 764–792; (j) A. Maiti, R. Yadav and L. Greb, *Adv. Inorg. Chem.*, 2023, **82**, 261–299.
- 4 Selected examples: (a) Z. Zong, Q. Zhang, S.-H. Qiu, Q. Wang, C. Zhao, C.-X. Zhao, H. Tian and D.-H. Qu, *Angew. Chem., Int. Ed.*, 2022, **61**(13), e202116414; (b) S. Neubacher and S. Hennig, *Angew. Chem., Int. Ed.*, 2019, **58**(5), 1266–1279; (c) E. Y. Zhou, H. J. Knox, C. Liu, W. Zhao and J. Chan, *J. Am. Chem. Soc.*, 2019, **141**(44), 17601–17609; (d) A. S. Walker, P. R. Rablen and A. Schepartz, *J. Am. Chem. Soc.*, 2016, **138**(22), 7143–7150; (e) W. Zhao and E. M. Carreira, *Angew. Chem.*, 2005, **117**(11), 1705–1707.
- 5 (a) B. Prajapati, M. D. Ambhore, D.-K. Dang, P. J. Chmielewski, T. Lis, C. J. Gómez-García, P. M. Zimmerman and M. Stępień, *Nat. Chem.*, 2023, **15**, 1541–1548; (b) P. Yang, M. J. Širvinskas, B. Li, N. W. Heller, H. Rong, G. He, A. K. Yudin and G. Chen, *J. Am. Chem. Soc.*, 2023, **145**(25), 13968–13978; (c) D. B. Diaz, S. D. Appavoo, A. F. Bogdanchikova, Y. Lebedev, T. J. McTiernan, G. dos Passos Gomes and A. K. Yudin, *Nat. Chem.*, 2021, **13**(3), 218–225; (d) I. Columbus, R. E. Hoffman and S. E. Biali, *J. Am. Chem. Soc.*, 1996, **118**(29), 6890–6896; (e) O. Golan, Z. Goren and S. E. Biali, *J. Am. Chem. Soc.*, 1990, **112**(25), 9300–9307.
- 6 Selected examples: (a) L.-P. Yang, L. Zhang, M. Quan, J. S. Ward, Y.-L. Ma, H. Zhou, K. Rissanen and W. Jiang, *Nat. Commun.*, 2020, **11**(1), 2740; (b) T. Suzuki, S. Yanaka, T. Watanabe, G. Yan, T. Satoh, H. Yagi, T. Yamaguchi and K. Kato, *Biochemistry*, 2019, **59**(34), 3180–3185; (c) D. W. Carney, K. R. Schmitz, J. V. Truong, R. T. Sauer and J. K. Sello, *J. Am. Chem. Soc.*, 2014, **136**(5), 1922–1929; (d) M. A. Campbell and J. Wengel, *Chem. Soc. Rev.*, 2011, **40**(12), 5680–5689; (e) S. J. Miller and R. B. Grubbs, *J. Am. Chem. Soc.*, 1995, **117**(21), 5855–5856.
- 7 IUPAC, *Compendium of Chemical Terminology*, 2nd edn (the “Gold Book”), 1997, Online corrected version: (2006–) “Lewis acid”, DOI: [10.1351/goldbook.L03508](https://doi.org/10.1351/goldbook.L03508).
- 8 The definition and role of confinement in homogeneous catalysis: B. Mitschke, M. Turberg and B. List, *Chem.*, 2020, **6**, 2515–2532.
- 9 Examples can be found scattered in the literature where the possibility of multiple adduct formation is raised as a result of directional anisotropy: (a) A. Poater, X. Solans-Monfort, E. Clot, C. Copéret and O. Eisenstein, *J. Am. Chem. Soc.*, 2007, **129**(26), 8207–8216; (b) A. Hamza, K. Sorochkina,



B. Kótai, K. Chernichenko, D. Berta, M. Bolte, M. Nieger, T. Repo and I. Pápai, *ACS Catal.*, 2020, **10**(23), 14290–14301; (c) L. Zapf, M. Riethmann, S. A. Föhrenbacher, M. Finze and U. Radius, *Chem. Sci.*, 2023, **14**(9), 2275–2288, Experimental structural studies: ; (d) I. D. Gridnev and T. Imamoto, *Acc. Chem. Res.*, 2004, **37**(9), 633–644; (e) P. Chaudhary, J. T. Goettel, H. P. A. Mercier, S. Sowlati-Hashjin, P. Hazendonk and M. Gerken, *Chem. - Eur. J.*, 2015, **21**(16), 6247–6256; (f) A. M. R. Hall, D. B. G. Berry, J. N. Crossley, A. Codina, I. Clegg, J. P. Lowe, A. Buchard and U. Hintermair, *ACS Catal.*, 2021, **11**(21), 13649–13659; (g) J. Bykowski, D. Turnbull, N. Hahn, R. T. Boeré, S. D. Wetmore and M. Gerken, *Inorg. Chem.*, 2021, **60**(20), 15695–15711, Structurally analogous boranes have been synthesized; however, neither the theoretical possibility of the multiple Lewis acidity phenomenon had previously been conceptualized nor had the multiple Lewis acidity phenomenon been perceived: ; (h) S. Toyota, M. Asakura, M. Ōki and F. Toda, *Bull. Chem. Soc. Jpn.*, 2000, **73**(10), 2357–2362; (i) M. Kemper, E. Engelage and C. Merten, *Angew. Chem., Int. Ed.*, 2021, **60**(6), 2958–2962, Finally, multiple adduct formation can be the result of multiple Lewis basicity. In this respect many prominent ligands can be found in the literature which may raise the issue of multiple Lewis basicity. Selected examples: ; (j) M. Kosugi, M. Kameyama and T. Migita, *Chem. Lett.*, 1983, **12**(6), 927–928; (k) A. Zapf, R. Jackstell, F. Rataboul, T. Riermeier, A. Monsees, C. Fuhrmann, N. Shaikh, U. Dingerdissen and M. Beller, *Chem. Commun.*, 2004, 38–39; (l) D. S. Surry and S. L. Buchwald, *Chem. Sci.*, 2010, **2**, 27–50; (m) Z. L. Niemeyer, A. Milo, D. P. Hickey and M. S. Sigman, *Nat. Chem.*, 2016, **8**, 610–617; (n) S. Zhao, T. Gensch, B. Murray, Z. L. Niemeyer, M. S. Sigman and M. R. Biscoe, *Science*, 2018, **362**, 670–674; (o) J. W. Lehmann, I. T. Crouch, D. J. Blair, M. Trobe, P. Wang, J. Li and M. D. Burke, *Nat. Commun.*, 2019, **10**, 1263, Additionally, there are some studies that have indicated the ability of certain Lewis basic ligands to have multiple bonding modes, but their NMR studies revealed that these scenarios are analogous to case B in Fig. 2 and can therefore be considered a single Lewis basicity. See for example: ; (p) M. T. Ashby, *J. Am. Chem. Soc.*, 1995, **117**(7), 2000–2007; (q) R. A. Widenhoefer, H. A. Zhong and S. L. Buchwald, *Organometallics*, 1996, **15**(12), 2745–2754; (r) J. A. S. Howell, M. G. Palin, P. McArdle, D. Cunningham, Z. Goldschmidt, H. E. Gottlieb and D. Hezroni-Langerman, *Inorg. Chem.*, 1991, **30**(25), 4685–4687; (s) S. H. Newman-Stonebraker, J. Y. Wang, P. D. Jeffrey and A. G. Doyle, *J. Am. Chem. Soc.*, 2022, **144**(42), 19635–19648.

10 M. Ōki, *The Chemistry of Rotational Isomers*, Springer, Berlin, Heidelberg, 1993, pp. 20–50.

11 (a) D. W. Stephan and G. E. Erker, *Angew. Chem., Int. Ed.*, 2010, **49**(1), 46–76; (b) T. Soós, *Pure Appl. Chem.*, 2011, **83**(3), 667–675; (c) D. W. Stephan, *Science*, 2016, **354**, aaf72296317.

12 (a) T. A. Rokob, A. Hamza, A. Stirling, T. Soós and I. Pápai, *Angew. Chem.*, 2008, **120**(13), 2469–2472; (b) A. Hamza, A. Stirling, T. A. Rokob and I. Pápai, *Int. J. Quantum Chem.*, 2009, **109**(11), 2416–2425.

13 É. Dorkó, M. Szabó, B. Kótai, I. Pápai, A. Domján and T. Soós, *Angew. Chem.*, 2017, **129**(32), 9640–9644. In this work for **I**, **II** and **III**, the reduction potentials determined in dichloromethane by CV: −2.1V, −2.0V, and −1.9V; the Gutmann–Beckett relative strength: 77%, 5%, and 4%; the relative hydricity (kcal mol<sup>−1</sup>, the lower energy value refers to weaker Lewis acidity): −15.3, −16.0, and −17.2.

14 (a) To understand the offset between some Lewis acidity scales and effort towards the unification of various Lewis acidity scales, see: P. Erdmann and L. Greb, *Angew. Chem.*, 2022, **134**(4), e202114550; (b) Further effort to develop a quantitative and Lewis-base-independent metric of Lewis acidity: A. R. Jupp, T. C. Johnstone and D. W. Stephan, *Dalton Trans.*, 2018, **47**(20), 7029–7035.

15 (a) U. Mayer, V. Gutmann and W. Gerger, *Monatsh. Chem.*, 1975, **106**, 1235–1257; (b) M. A. Beckett, G. C. Strickland, J. R. Holland and K. S. A. Varma, *Polymer*, 1996, **37**(20), 4629–4631.

16 We also calculated the fluoride ion affinities of the rotamers of Lewis acid **I** as fluoride is the hard-type Lewis base analog of the hydride. This study showed that the hard-type ligand neither changed the trend nor affected the energy differences between the atropisomeric dative adducts (ESI Section 10†). For a related analysis demonstrating that fluoride, hydride, and hydroxide affinities follow the same trends and relative energy differences towards Ar<sub>2</sub>CH<sup>+</sup> cations, see: C. Schindeler, K. N. Houk and H. Mayr, *J. Am. Chem. Soc.*, 2002, **124**, 11208–11214.

17 Recent evidence suggests that the conformational stabilization in certain macrocycles is primarily due to intramolecular hydrogen bonding, which acts as a “structural pin”: S. D. Appavoo, N. W. Heller, C. T. van Campenhout, G. J. Saunders and A. K. Yudin, *Angew. Chem., Int. Ed.*, 2024, **63**(28), e202402372.

18 <sup>19</sup>F–<sup>1</sup>H HOESY studies towards establishing hydrogen–fluorine internuclear distances in fluorinated organic compounds and adducts: (a) G. Ciancaleoni, R. Bertani, L. Rocchigiani, P. Sgarbossa, C. Zuccaccia and A. Macchioni, *Chem. - Eur. J.*, 2015, **21**(1), 440–447; (b) Y. Lingscheid, M. Paul, A. Bröhl, J.-M. Neudörfl and R. Giernoth, *Magn. Reson. Chem.*, 2018, **56**(2), 80–85; (c) L. Dewis, R. Crouch, D. Russell and C. Butts, *Magn. Reson. Chem.*, 2019, **57**(12), 1143–1149; (d) Q. M. Dang, J. H. Simpson, C. A. Parish and M. C. Leopold, *J. Phys. Chem. A*, 2021, **125**(42), 9377–9393.

19 For hydrogen bond *J*<sub>HF</sub> values: (a) G. N. M. Reddy, M. V. V. Kumar, T. N. G. Row and N. Suryaprakash, *Phys. Chem. Chem. Phys.*, 2010, **12**, 13232–13237; (b) D. Kumari, S. Hebbar and N. Suryaprakash, *Chem. Phys. Lett.*, 2012, **525**, 129–133; (c) S. R. Chaudhari, S. Mogurampelly and N. Suryaprakash, *J. Phys. Chem. B*, 2013, **117**(4), 1123–1129.

20 On through-space <sup>19</sup>F–<sup>19</sup>F couplings in multifluorinated organic compounds and adducts: (a) L. Ernst and



K. A. Ibrom, *Angew. Chem., Int. Ed.*, 1995, **34**(17), 1881–1882;  
(b) F. B. Mallory, C. W. Mallory, K. E. Butler, M. B. Lewis, A. Q. Xia, E. D. Luzik, L. E. Fredenburgh, M. M. Ramanjulu, Q. N. Van, M. M. Franel, D. A. Freed, C. C. Wray, C. Hann, M. Nerz-Stormes, P. J. Carroll and L. E. Chirlian, *J. Am. Chem. Soc.*, 2000, **122**(17), 4108–4116;  
(c) J.-C. Hierso, *Chem. Rev.*, 2014, **114**(9), 4838–4867; (d) H. W. Orton, H. Qianzhu, E. H. Abdelkader, E. I. Habel, Y. J. Tan, R. L. Frkic, C. J. Jackson, T. Huber and G. Otting, *J. Am. Chem. Soc.*, 2021, **143**(46), 19587–19598.

21 Selected EXSY applications in coordination chemistry: (a) A. Pastor and E. Martínez-Viviente, *Coord. Chem. Rev.*, 2008, **252**(21–22), 2314–2345; (b) M. B. Schmid, K. Zeitler and R. M. Gschwind, *Angew. Chem., Int. Ed.*, 2010, **29**(49), 4997–5003; (c) K. A. D'Angelo and M. S. Taylor, *J. Am. Chem. Soc.*, 2016, **138**(34), 11058–11066.

22 H. Iwamura and K. Mislow, *Acc. Chem. Res.*, 1988, **21**(4), 175–182.

23 Z. Liu, Z. Zhang and R. O. Ritchie, *Adv. Funct. Mater.*, 2020, **30**(10), 1908121.

24 (a) X. Wu, R. M. Witzig, R. Beaud, C. Fischer, D. Häussinger and C. Sparr, *Nat. Catal.*, 2021, **4**(6), 457–462; (b) T. A. Schmidt and C. Sparr, *Acc. Chem. Res.*, 2021, **54**(12), 2764–2774.

